Mustansiriyah Journal of Pure and Applied Sciences, Print ISSN: 2957-9910. Online ISSN: 2957-9929, Vol. 4, No. 3, 2026, Pages 92-104
DOI: 10.47831/mjpas.v4i3.448

MUSTANSIRIYAH JOURNAL OF PURE AND APPLIED SCIENCES

MJPAS

Journal homepage:
https://mjpas.uomustansiriyah.edu.iq/index.php/mjpas

RESEARCH ARTICLE - PHYSICS

Enhancement the sensitivity and temporal response of porous silicon gas sensor via integrating gold nanoparticles

Abeer Ghalib Hadi[1], Alwan M. Alwan [2], Ali A. Yousif [1*]

[1]Mustansiriyah University, College of Education, Physics Department, Iraq.
[2] University of Technology, School of Applied Science, Baghdad, Iraq.
[*] Corresponding author: aliyousif73@uomustansiriyah.edu.iq

Article Info.

Article history:

Received
13 June 2025

Accepted
9 September 2025

Publishing
30 September 2026

Abstract

In this research, two specific types of planner mode room temperature gas sensors involve a bare (PS), and PS/AuNPs were synthesized and tested to detect low NO_2 gas concentrations from 10ppm to 40ppm. The bare PS was prepared by laser assisted electro chemical etching of N type (100) silicon wafer. The results showed, that the sensitivity of PS sensor was 7.5% at gas concentrations of 10 ppm and 13.1% at gas concentrations of 40 ppm. While for AuNPs/PS sensor, the sensitivity was increased steadily from 55.6% at gas concentration of 10ppm to 83.6% at gas concentration of about 40ppm, also, relationship between the sensitivity and the gas concentration is nearly linear relationship without saturation effects. The temporal response Rst and Rct of PS sensor is about 96 sec and 122 sec and for AuNps/PS is about 58 sec and 82 sec respectively. The improvement of Rst and Rct in AuNPs are about 65% and 49% respectively. This significant improvement in AuNPs/PS sensor, in sensing process, is due to the thermal conductivity of AuNPs in additional surface area of AuNPs

The official journal published by the College of Education at Mustansiriyah University

Keywords*:* porous silicon, Au nanoparticles, laser assisted electro chemical etching, NO_2, planner mode, gas sensor

Introduction

The Porous silicon (PS), is a network of crystalline Si that resembles a sponge. It has several nanoscale forms (such as trenches, mud, columns, and pores) with nanoscale [1][2]. This material gained attention only in 1990 when Canham discovered its intrinsic photoluminescence (PL) at room temperature, despite the fact that Uhler unintentionally discovered it in 1956 during an electrochemical experiment [3][4]. Because of its remarkable characteristics, nanostructure-sized porous silicon has a high surface-volume ratio and strong visible photoluminescence, making it suitable for a wide range of applications [5]. PS is defined by its thickness, internal surface (considering the pore surfaces), morphology (shape and pore size), and porosity (volumetric percentage of voids inside PS), as it can display a variety of morphologies and typical pore sizes. According to the predominant pore diameter (d), the PS structures are divided into three categories: macroPS ($d > 50$ nm), mesoPS (2 nm $< d < 50$ nm), and microPS ($d \leq 2$ nm) [6][7]. The doping type, orientation, and ECE variables of the silicon (Si) substrate have a significant impact on the pore characteristics of PS[8]. It is a semiconductor material with unique physical and chemical properties. Surface passivation is essential for defining the physical, chemical, and electrical characteristics of PS structures. The PS is extremely reactive owing to its high surface-to-volume ratio. The surface can be stabilized, carrier recombination can be altered, and the optical and electrical properties of the material can be customized by carefully managing this process, which is usually accomplished by the development of oxide or organic layers. PS may be optimized for a variety of applications, such as photonic devices, sensors, and healthcare systems, owing to its controlled surface alteration. [6]and[7]. A crucial role is played by knowledge of the pore size, distribution, surface chemistry, and reliance on manufacturing circumstances in all PS applications. A link between the PS morphology and preparation parameters, as well as the correlation between the measured physical attributes and PS film morphology, is required. Macropore formation mainly depends on temperature, anodizing solution, and substrate properties such as crystal orientation and doping [9] PS can be prepared by several techniques, including metal-assisted, stain, electrochemical, and photo-

electrochemical etching (PECE), with PECE being a cost-effective method for morphology control [2]. Key parameters such as etching current, HF concentration, and substrate orientation are critical for nanostructure formation in n-type silicon [10]. Gold nanoparticles (AuNPs) are of interest because of to their low toxicity[11] , and critical properties [12]. Its initial surface or interface turns into a semi-stable end of silicon and hydrogen following the silicon etching process and creation of porous silicon [13] Surface structures can deteriorate as a result of the naturally oxidation process of metastable hydro silicon in the ambient environment. Furthermore, this implies that a post-formation treatment is required to passivate the high-density defect states, and the PS surface must be modified [14]. The interaction between silicon and gold is frequently utilized in electrical devices to regulate their resistivity and lifespan [15][16]. AuNPs were created by combining self-assembly and chemical e-beam lithography methods [17][18],or via the electron beam evaporation method and ion reduction. A variety of gold and silver nanoparticle sensing devices have been developed to increase the sensitivity[19] Therefore, employing multifaceted PS layers is regarded as one of the key scientific ideas to enhance sensor performance as it increases the sensor's overall surface area [20]. Mhamdi, H., et al prepared PS synthesized via stain etching technique to detect low concentrations of NO_2 at room temperature, the synthesized structures were studied the gas sensing properties and structural properties. The sensors showed considerable sensitivity to low NO_2 concentrations, with a response time of up to 45 seconds [21]. Azaiez, Khaoula, et al presented a nitrogen dioxide gas sensor based on porous Morphology, structural were investigated using scanning electron microscope (SEM), X-ray diffractometer (XRD) and offering improved sensitivity, selectivity, and cost-efficiency. The sensor was prepared using meso-porous silicon (meso-PS) films and tested at room temperature with Al electrodes. The sensor showed high normalized response, good repeatability, fast response, and selectivity for NO_2 , making it suitable for low-power devices [22]. Sainato et al.'s 2015 study showed gold-decorated porous silicon can be used as high-performance Chemi-transistor sensors for NO_2 detection at sub-ppm levels, with stable operation for up to 48 hours [23]. L&y-CXment, C., et al prepared the PS through photoelectrochemical etching, resulting in controlled corrosion under light and anodic polarization in HF. Synthesized structures were studied morphologically and structurally by SEM, XRD [24]. The main objective of this research is to improve the performance of gas sensors based on a porous silicon layer by incorporating gold nanoparticles. This is based on the distinct thermal properties of gold nanoparticles, as well as their high surface area. Increasing the sensitivity to detecting NO_2 gas, in addition to increasing the detection speed, is the focus of this study.

Experiments

PS formation

An n-type silicon wafer was used as the research material in this study. It had a resistivity of 20 Ω · cm and was 500 ± 10 μm thick with (100) orientation. Photoelectrochemical etching (PECE) was used to generate PS substrates using a Teflon cell. After cutting the silicon wafer into 1.5 cm × 1.5 cm pieces, it was cleaned using a solution made of ethanol C_2H_6O (99%) and hydrofluoric acid (HF) 49% in a 1:10 ratio. After being submerged in deionized water, the samples were stored in methanol-prepared containers (CH_3OH). To remove organic and oxide layers as well as other contaminants, the silicon layer was cleaned [25]. Once the samples were cleaned, they were placed in a Teflon cell with a 1:1 ethanol/hydrofluoric acid (HF) ratio and etched using an ammeter. With current 20 mA and the etching time is 25 min. We employed an auxiliary continuous laser with a wavelength of 632 nm and the laser power density is 100W/cm^2 to complete the etching process. An auxiliary laser with a wavelength of 632 nm was employed to complete the etching process. The etching setup is illustrated in Fig. 1

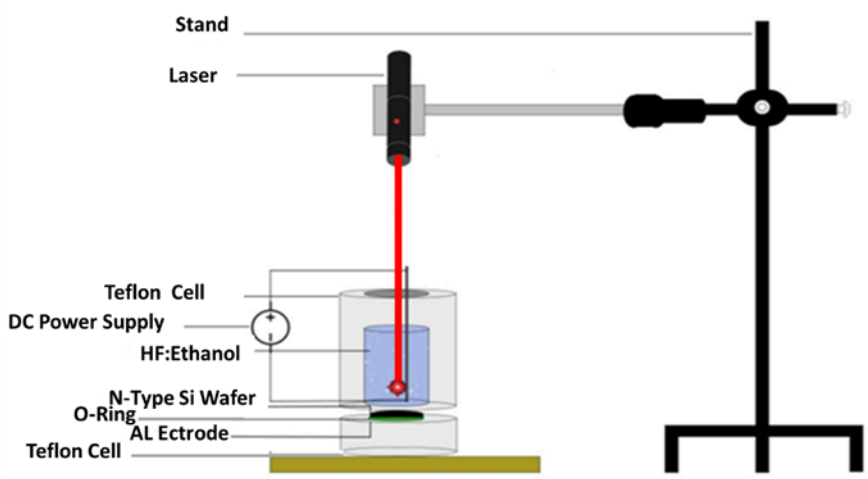

Figure 1: Demonstrated the laser assisted electrochemical process for PS

A gravimetric method was employed to compute the porosity of the PS layer. The sample was weighed before (m_1) and after (m_2) etching, dipped in a 1M NaOH solution at room temperature to remove the porous layer, and weighed again (m_3) [26]. The porosity of the porous silicon sample was calculated using equation. 1 [9].

$$P = \frac{m1-m2}{m1-m3} \times 100\ \% \qquad (1)$$

Preparation the AuNPs

Gold nanoparticles were manufactured by dissolving the concentrated gold salt $HAuCl_4$ in deionized water. The solutions were placed on a magnetic stirrer until they were homogeneous and turned to yellow color, as shown in Fig. 2.

Figure 2: The process of preparing the $HAuCl_4$ solution.

Preparation of AuNPs/PS substrate

After the substrate PS was prepared, the modified AuNP/PS gas sensor substrate was created by dipping fresh PS in $HAuCl_4$ at a concentration of 10^{-3} M for approximately 2 min. The necessary solution concentration was calculated using equation 2 [27].

$$\text{Molarity} = \frac{\frac{W}{M.Wt}}{V} \qquad (2)$$

where W (g) is the weight of $HAuCl_4{:}3H_2O$, M is the volume of the dissolved solution, and the weight of $HAuCl_4{:}3H_2O$ is approximately 393.83 (gm/mole). The following reactions, respectively, determine how Au NPs formed by the reduction of Au^{+3} ions with dangling bond groups (Si-Hx) undergo ion reduction deposition inside the PS structure interface as exposed in equations 3 and 4. [28] [29] [30] :

$$2Si + 6HF \rightarrow H_2SiF_6 + 4H^+ + 4e^- \qquad (3)$$

$$Au^{3+} + 3\,e^- \rightarrow Au\ NPs \qquad (4)$$

Gold nanoparticles AuNPs were deposited on porous silicon samples by immersing them in gold salt solutions, which were subsequently identified as gas sensors. As shown in Fig. 3a. The sensor fabrication process involves a metallization process through thermally deposition an aluminums electrode on the substrate's surface, as illustrated in Fig. 3b.

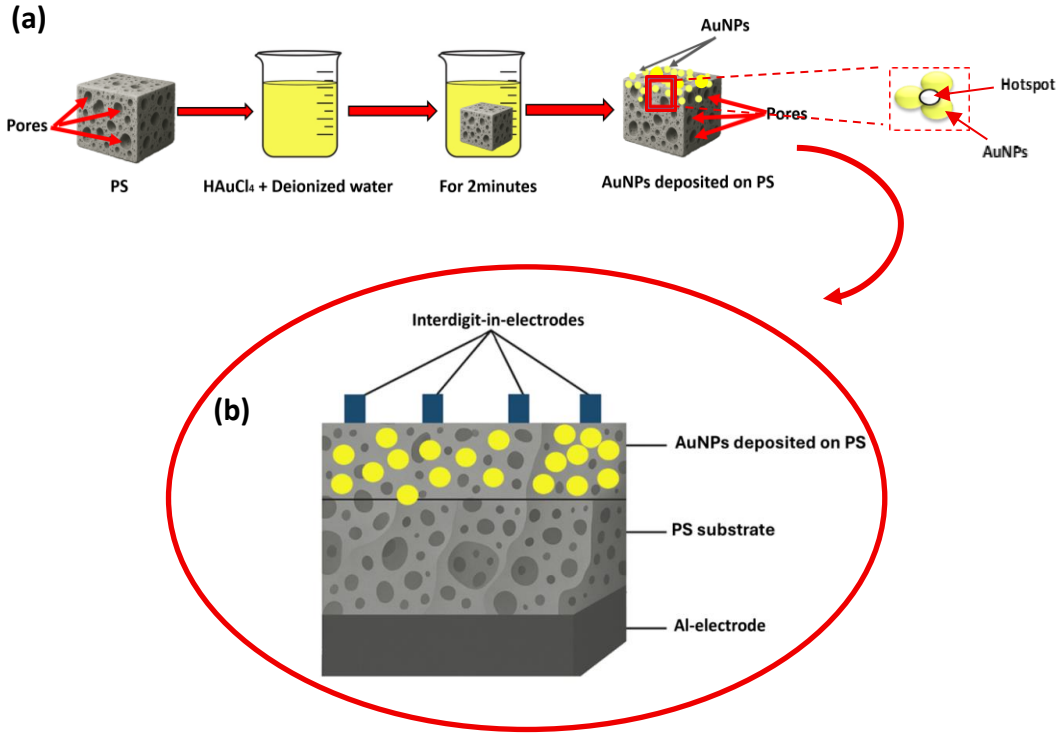

Figure 3: a) illustrates the steps of incorporating AuNPs on PS layer, b) gas sensor metallization

Gas sensing

The sensitivity of the AuNP-implanted PS bilayer gas to NO_2 was assessed using gas sensor testing equipment, including a stainless-steel chamber cavity with a capacity of 10× 10 × 10cm^3 as shown in Fig. 4. Prior to the detection, the basal pressure was approximately 1 mbar. Two precision valves were used for the gas in and out of the chamber at room temperature. Using a rotational pump to obtain a base pressure of approximately 1mbar, the chamber was evacuated early. Every measurement was performed at room temperature several times, and the average reading was obtained for the gas-sensing procedure.

The sensitivity (S) of the planar-mode gas sensors of bare PS and modified AuNPs/PS is given by the ratio of change in resistance (R with gas -R without gas) to Ra, equation 5 [31]

$$S = \frac{Rg - Ra}{Ra} \times 100\% \qquad (5)$$

where: Rg refer to the resistance with gas, Ra is the resistance without gas

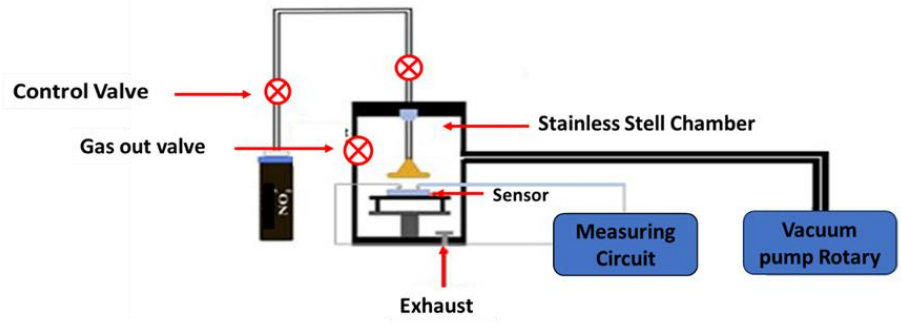

Figure 4: The gas sensing set up

Results and discussions

The AFM images of bare PS and modified Au NPs/Ps are shown in Figs. 5(a) and (b) and Figs. 6(a) and (b). Both figures illustrate the formation of pores, presenting 3D images in this format. Fig. 5(a) displays the estimated average roughness Sq (Root Mean Square Roughness) of the PS sample at 10.538 nm, while the average roughness Sq of the AuNPs/PS sample is 18.1742 nm. The surface changed, becoming rougher following the deposition of gold nanoparticles, as shown in Fig. 6a .The shape of the dangling bond groups affected the growth of the AuNPs[32]. Because PS layer deposition varies depending on the density and location of the growth sites (Si–Hx time), the structural characteristics of the generated AuNPs nanoparticles are altered at the fixed surface morphology of the bare PS layer, have column sizes around (30-90) nm is the highest of the column size distribution with 93%, as shown the histogram in Fig. 5b, while highest of the pore size distribution at 98% for AuNPs/PS and it has column sizes around (40-100) as shown in Fig. 6(b).

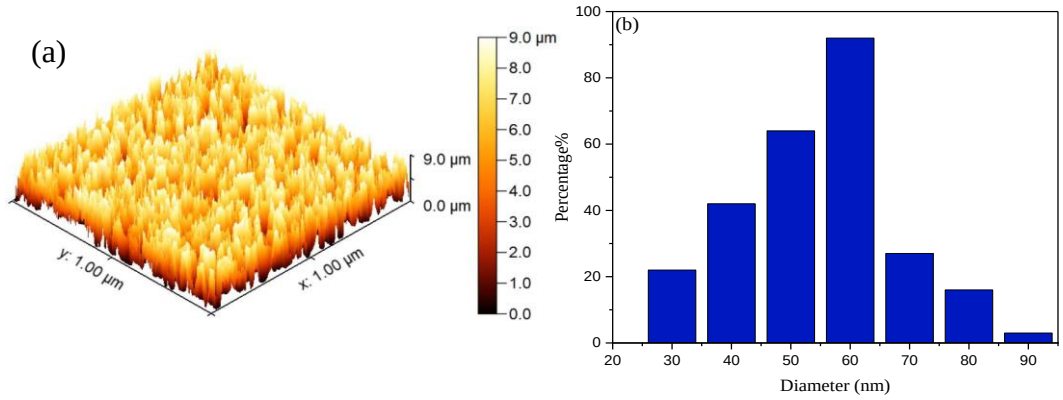

Figure 5: (a) 3D of Psi, (b) histogram of column sizes of bare PS.

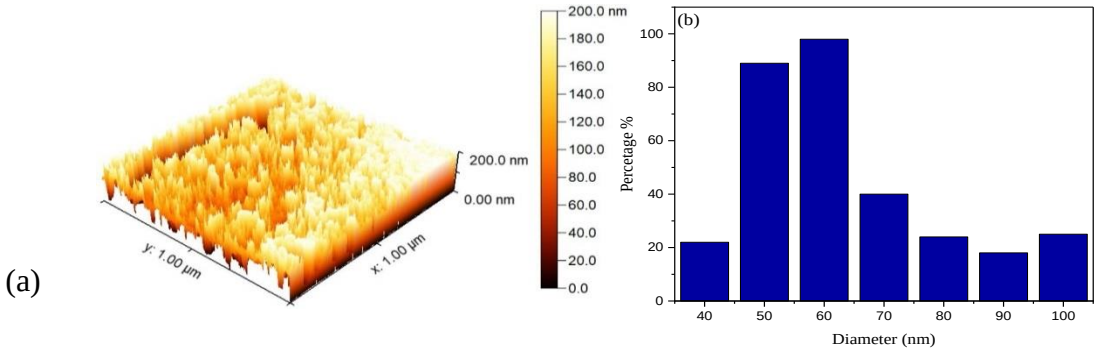

Figure 6: (a) 3D image of AuNPs/PS, (b) histogram of modified AuNPs/PS

The morphological properties of the bare PS and modified AuNPs/PS are illustrated in Fig. 7 and 8, respectively. Fig. 7 (a) and (b) show the appearance of the PS layer on the surface. According to the FE-SEM image, the surface of bare PS consists of pores that are part of a network of structures that resemble macropores. Approximately systematic, nearly square-shaped, or close to the shape of the stars and distributed on the surface, these pores can connect with one another; thus, the connected pores overlap with each other, making some pores appear wider than others. The statistical distribution of the pore diameters indicates that they fall between 1.297 and 1.636 µm, as shown in Fig.7a. The morphological characteristics of the bare PS and modified AuNPs were evident. The pore has columns and forms with almost the same depth and arrangement, according to the cross-section of the image displayed in Fig. 7b. The depth of the range was approximately 92.59 µm. After depositing the Au NPs on the surface of the PS, the distribution of the pore diameters

indicated that they fell between 1.080 and 1.521 µm, which means that the pore diameter decreased after the addition of AuNPs. As for the cross-section of modified AuNPs/PS, the layers of gold nanoparticles range from 7.625 µm to 15.53 µm, as shown in Fig.7b. In Fig. 8a, shown with a magnification of 500 nm, the grain size of AuNPs ranges from 48.57 nm to 71.91 nm due to the presence of an aggregation mechanism. The AuNPs were roughly round in shape. Fig.8a, at a magnification of 3 µm, illustrates how they agglomerated with a high density of aggregation. Certain areas of the substrate are empty of the generated Au NPs, and the surface is not entirely covered by them. Because of the dangling bonds of the Si-Hx groups' random distribution throughout the porous surface and the uncontrolled mobility of the gold ions, as previously mentioned, it is more difficult to deposit metallic nanoparticles within a certain size. The pore size of the modified AuNPs/PS was between 1.080 and 1.521 µm, which means that after adding AuNPs, the size of the pores decreased because some Au NPs were deposited on the surface and inside the pores.

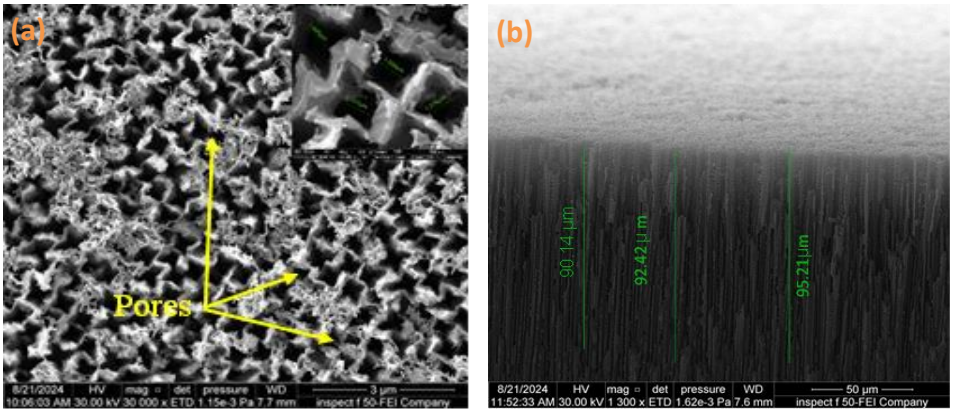

Figure 7: (a) FE-SEM images of bare PS with magnification3µm, 500 nm sequentially and (b) cross-sectional image

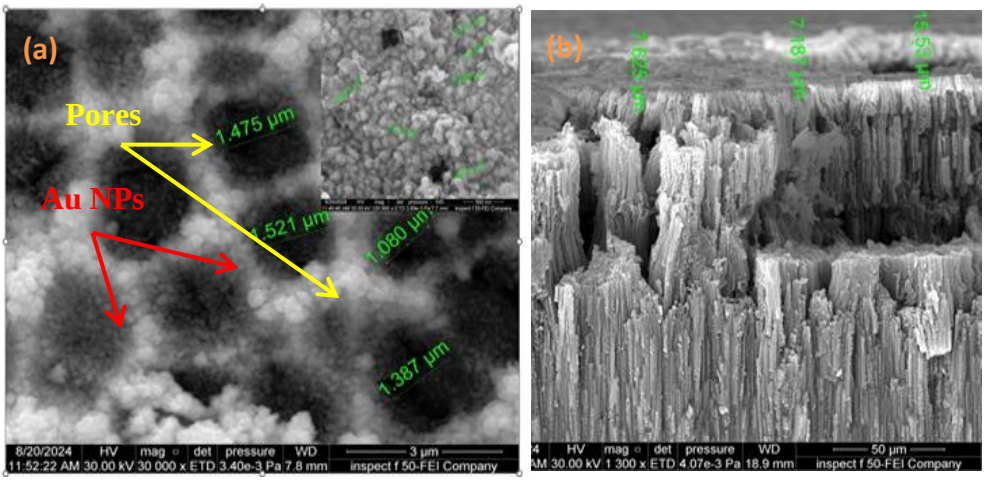

Figure 8: (a) FE-SEM images of modified AuNPs/PS with magnification 3µm, 500 nm sequentially and (b) cross-sectional image.

The value of porosity of the bare PS layer was 69 % of the sample volume. This degree of porosity is appropriate for sensor devices that use porous silicon because open pores enhance the effective surface area and sensing capabilities. Energy Dispersive Spectroscopy (EDS) measures the distinctive X-rays emitted by a material emits in order to determine the chemical elements present in it. The exact details regarding the composition of the sample and the proportions of various elements are provided in this analysis. To identify any contaminants or chemical alterations in the

sample, EDS was used to verify the existence of the deposited components. From Fig. 9a, The EDS examination revealed fewer peaks for oxygen (O) and a primary peak for silicon (Si)in the PS. The outcome shows that silicon constitutes the majority of the sample, with a trace quantity of oxygen probably present because of air exposure or etching procedures. The presence of Si, Au, and O in the modified AuNP/PS sample is shown in Fig. 9b. The presence of oxygen on the modified AuNP/PS sample indicates the oxidation of Si, while the presence of Si is ascribed to the Si substrate.

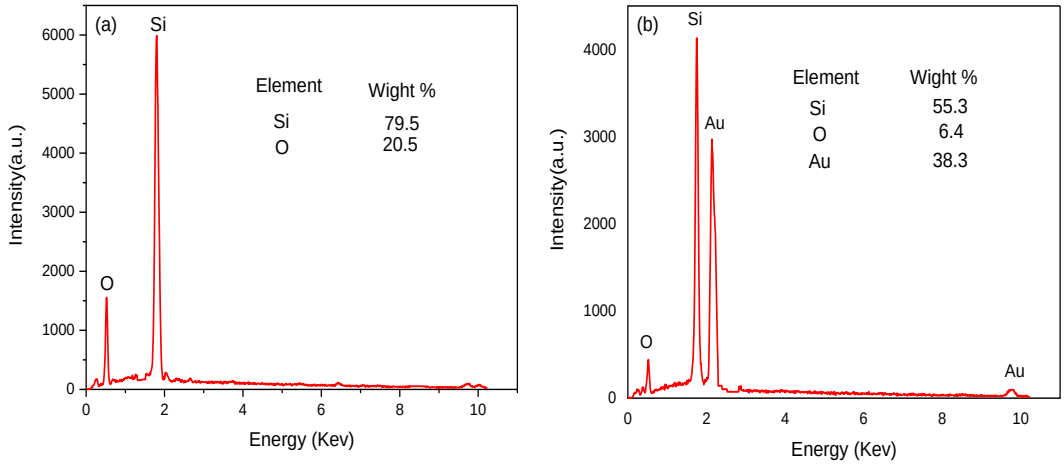

Figure 8: The EDX analysis of (a) bare PS and (b) modified AuNPs/PS substrate.

The structural properties of bare PS and modified AuNPs/PS substrates, were investigated by study the diffraction patterns (XRD) as shown in Figures 10a and b respectively. According to equation 6 (Scherrer equation)[33][34]The crystallite size of porous silicon was 18.9 nm, and it was demonstrated that the bare PS layer maintained its crystal structure in the (100) plane at a diffraction angle (2θ) of approximately 69.52°.

$$L = \frac{0.9\lambda}{\beta cos\,\theta} \qquad (6)$$

Where L is crystallite size, λ=1.5405 A° is the XRD wavelength, β is FWHM, and θ is diffraction angle.

In Fig. 8a, the appearance of two peaks at 33.40° and 62.19° can be attributed to surface structures that can deteriorate due to the spontaneous oxidation of the hydrogenated PS in the surrounding environment. Sometimes this requires PS surface modification to extinguish and suppress high-density and high-density defect states[14] [35]

These additional peaks can be to the formation of silicon oxides (SiO_x) on the pore walls as a result of the spontaneous oxidation of quasi-stable hydride-terminated silicon. PS produced by electrochemical etching is initially covered with a hydrogen-terminated surface (Si–H), which provides temporary resistance to oxidation. Furthermore, when the PS is exposed to air, the bonds gradually break, leading to the formation of SiO_2, or semi-crystalline phases, which exhibit characteristic diffraction peaks at these positions.

The gold nanoparticles in the (111), (200), (220), (311), and (222) planes were responsible for the Bragg reflections at diffraction angles 38.70°, 44.94°, 64.76°, 77.93°, and 82.29°, respectively[36]. The AuNPs have an average crystallite size of 8.092 nm. The Au NPs were at the (111) plane, as shown by the main angle of 38.70°. had a crystallite size of approximately 4.5 nm. The XRD study of PS incorporated with gold revealed unexpected peaks at 33° and 62° (2θ) in addition to the silicon and gold peaks. The deposition process produces several overlapping effects that can account for these extra peaks. First, the residual stress of the gold layer on the porous silicon surface modified the crystal lattice, causing the peak positions to change. Furthermore, peak broadening and

additional shifting were caused by the nanocrystalline structures of both materials. Chemically, the development of Au–Si interfacial phases and surface oxidation (SiO_x) during immersion are factors that may cause new or displaced peaks. Another factor influencing the XRD pattern is the interaction between Au^{3+} ions and Si–H bonds on the pore walls [37]. The results obtained suggest that more research should be conducted to determine how the structural and electrical properties of PS are affected by the parameters of gold deposition, such as particle size, thickness, and distribution. A better understanding of the behavior of the material at the nanoscale would also come from a thorough investigation of the quantum confinement effects caused by the smaller crystallite size .Because gold deposition significantly increases the surface area, chemical activity, and electrical sensitivity, it is advisable to investigate the possible use of gold-decorated porous silicon in gas sensor systems. The evaluation of the sensitivity, selectivity, reaction time, and stability of these nanostructured sensors towards different target gases should be the focus of future research. Such research could lead to the creation of extremely effective, stable, and fast-response gas-sensing systems for industrial and environmental monitoring. It is evident from table2 analysis that the interplanar spacings the vary widely, ranging from 0.23 2.3 A°. This variance is a result of the residual strain in the crystal lattice caused by surface chemical interactions and deposition. The XRD investigation provides additional confirmation of this, revealing shifts and distortions in the peak positions that point to structural deformation caused by strain.

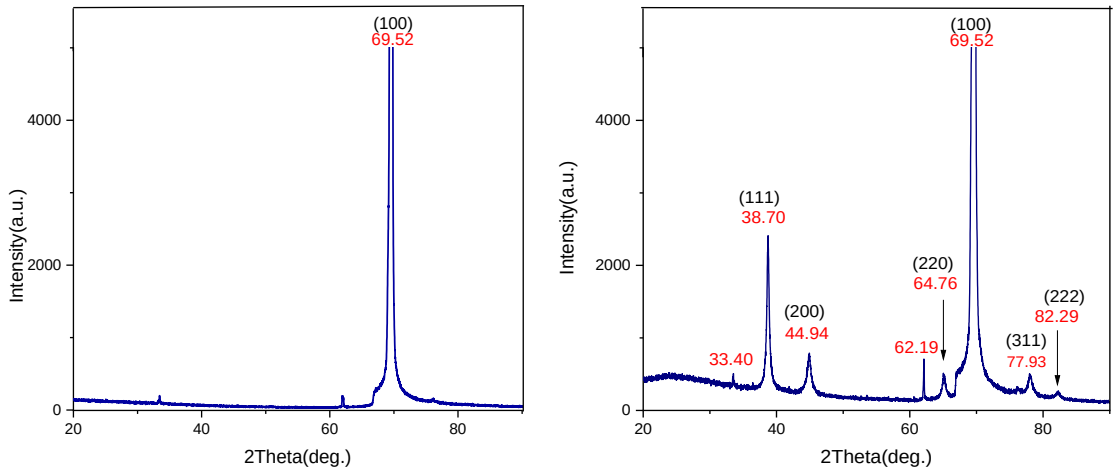

Figure 10: (a) shows the XRD pattern of PS deposited with $HAuCl_4$ at a concentrations10^{-3}, (b) shows the XRD pattern of AuNPs/PS deposited with $HAuCl_4$ at a concentration of 10^{-3}

Table 1 illustrations the structural parameters of PS and modified AuNPs/PS

Sample	2 Theta(deg.)	FWHM (deg.)	plane	d-spacing A°	D (nm)	
PS	69.52	5.2970	100	1.3506	18.9	
AuNPs/PS	38.70	2.2660	111	0.2328	4.5	average 8.092
	44.94	0.6143	200	2.015	13.99	
	64.76	3.1412	220	1.4384	2.99	
	77.93	0.7368	311	1.2248	13.86	
	82.29	2.0278	222	1.1707	5.12	

The specific surface area (S.S.A) of nanoparticles is a very important parameter for determining their advantage limit for sensing applications. The value of S.S. A was calculated using equation. 7 [38].

$$S.S.A = \frac{6000}{\rho D} \qquad (7)$$

where (D) and ρ represent the crystalline size and density of gold, respectively. the value of the crystalline size and the S.S.A is about 4.5 nm and 69 m^2/gram

Mechanism of NO2 gas sensing

The adsorbed oxygen was produced via the following reactions equations. (8-10). [21]

$$O_2(gas) \rightarrow O_2(ads) \quad (8)$$
$$O_2(ads) + e^- \rightarrow O_2^-(ads) \quad T < 100\ C^o \quad (9)$$
$$O_{2-}(ads) + e^- \rightarrow 2O_2^-(ads) \quad 100C^o < T < 100\ C^o \quad (10)$$

When nitrogen dioxide (NO_2) passes through to a porous silicon (PS) sensor, the gas molecules im mediately adsorb onto the surface and capture silicon electrons.

Furthermore, chemisorbed oxygen species (such as O_2 and O^-) that are already present on the surfac e interact with these NO_2 molecules. reaction equations.11, 12, 13demonstrates how this interaction increases the conductivity and resistance of the sensor, allowing for the detection of NO_2 [39] .

$$NO_2(gas) + e^- \rightarrow NO_2^-(ads) \quad (11)$$
$$NO_2(ads) + 2O^-(ads) + 2e^- \rightarrow NO_2^-(ads) + 2O_2^-(ads) \quad T < 100\ C^o \quad (12)$$
$$NO_2(gas) + O^-(ads) + 2e^- \rightarrow NO_2^-(ads) + O_2^-(ads) \quad 100C^o < T < 100\ C^o \quad (13)$$

The Fig. 11a, b, illustrates the temporal response (response time Rst and recovery time Rct) of bare PS and gold nanoparticles modified porous silicon (AuNps/PS) gas sensors respectively. From this figure, the values of Rst and Rct for the bare PS gas sensor are approximately 96 and 122 s, respectively. For the AuNps/PS gas sensor, the values of Rst and Rct were lower than those of the bare PS gas sensor at approximately 58 s and 82 s, respectively. The relative improvements in Rst and Rct after incorporation AuNPs were approximately 65% and 49%, respectively. This significant improvement in both the response and recovery times after the introduction of gold nanoparticles into the porous silicon layer is due to the very high thermal conductivity of the gold particles deposited inside the porous silicon skeleton. This lowers the temperature inside the pores of the PS and thus reduces the condensation rate of gas molecules inside the pores, which accelerates the degassing process. Although the crystalline silicon sample used is of the donor type, owing to the etching process, the majority of the electric charge carriers are depleted; therefore, the electrical behavior of the PS produced from the donor-type sample is that of the acceptor-type silicon sample [40].

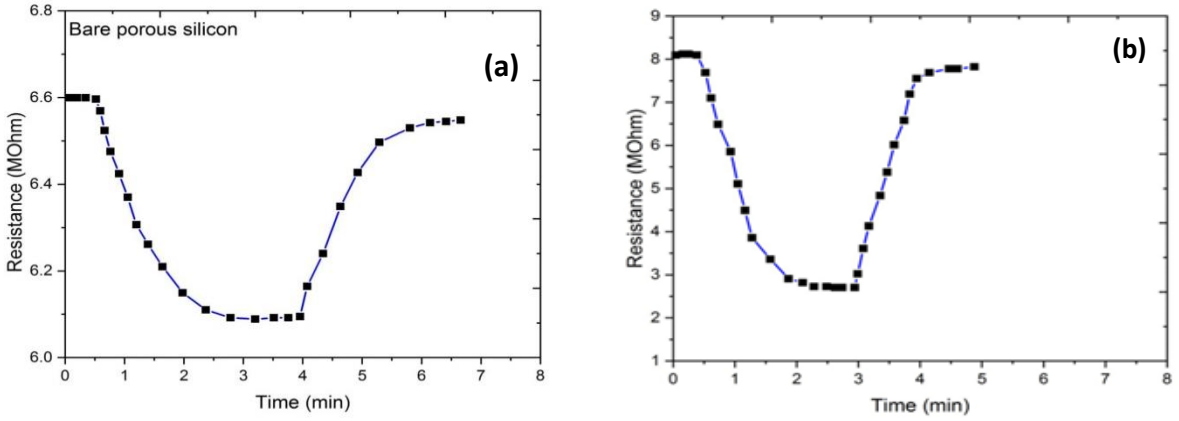

Figure 11: illustrates the temporal response of a) bare porous silicon and b) modified AuNPs/PS gas sensors at a fixed gas concentration of 10ppm

Figures 12a, b, illustrates the response of both sensors, the bare PS and AuNps/PS gas sensors as a function to gas concentration froı ı 10 to 40 ppm. From these sensors, it's easily to recognize the

reproducibility of the sensor, where the response and recovery times still fixed relatively in spite of the increasing of the gas molecules condensation. The lack of significant changes in response time and recovery time indicates that saturation has not occurred, especially after the deposition of gold nanoparticles this positive behavior will enhance the sensor's efficiency this agreement with [41].

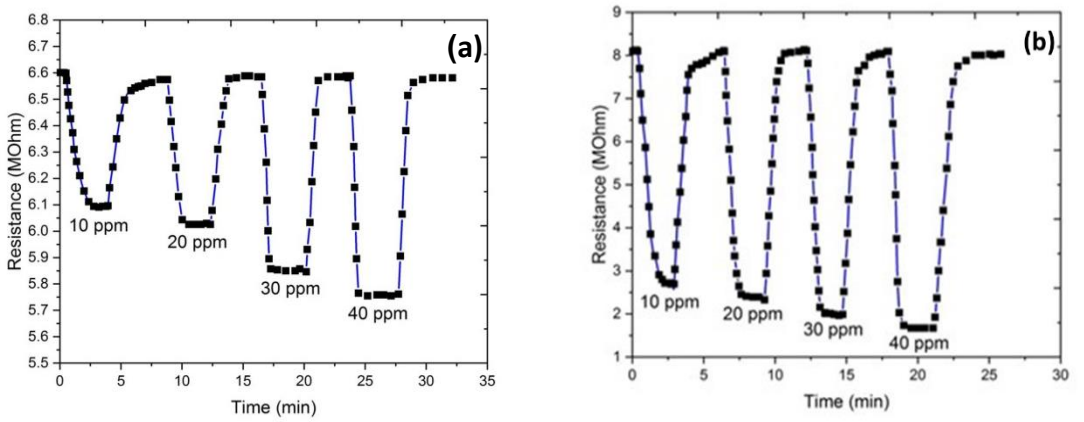

Figure 12: a, b illustrates the temporal response (response time Rst and recovery time Rct) of bare PS and gold nanoparticles modified porous silicon (AuNps/PS) gas sensors respectively with different concentration of gas (10 ppm,20 ppm,30ppm and 40 ppm)

For the bare PS gas sensor, Fig.13a, the sensitivity of the sensor increased with increasing gas concentration inside the sensing chamber. The sensor's sensitivity ranged from 7.5% at low gas concentrations of 10 ppm to 13.1% at high gas concentration of 40 ppm. These low sensitivity values are due to the low adsorption rate of gas molecules within the PS layer, which causes the dielectric constant of the porous silicon layer to remain significantly unchanged; thus, no significant change occurs in the electrical resistance of the sensor after the introduction of gas molecules. For the modified AuNps/PS gas sensors Fig.13b, the sensitivity increased with the gas concentration inside the chamber, but with a large amount. The sensitivity ranges from 55.6% at low gas concentration of 10ppm to 83.6% at high gas concentration of about 40ppm this significant increase in sensitivity in the sensor after adding gold nanoparticles is due to the increased adsorption rate of gas molecules resulting from the increased surface area of the sensor. This surface area originates from both the surface area of the porous silicon and that of the gold nanoparticles. AuNPs also have a significant effect on the dielectric constant of the porous silicon layer, thereby altering the electrical resistance of the sensor. The relative improvement in gas sensor sensitivity at constant gas concentration (S% with gas _ S% without gas / S% without gas) is approximately 500%. The relationship between the sensitivity of the sensor and the gas concentration after adding gold nanoparticles was as close as possible to a linear relationship without saturation effects. This makes the sensor efficient at responding to high concentrations of gas molecules. For sensors without gold nanoparticles (bare PS), the relationship between the sensor sensitivity and gas concentration tends to saturate, especially at high concentrations. This behavior reduces the ability of the sensor to detect high concentrations.

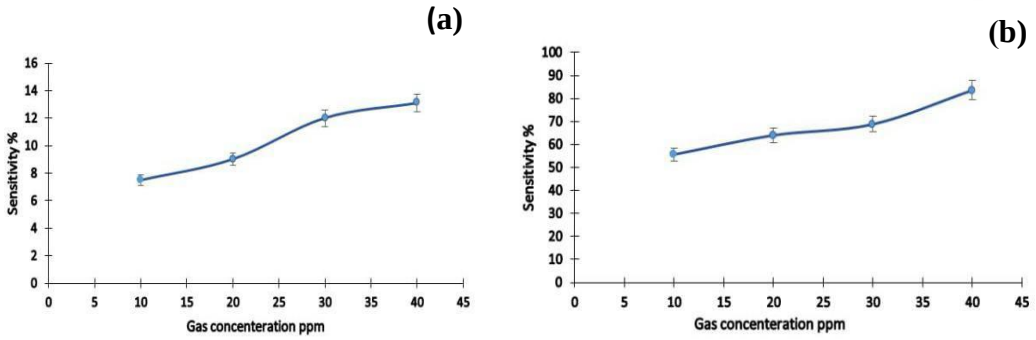

Figure 13: Displays the sensitivity of the a) bare PS, b) modified AuNps/PS gas sensors as a function to concentration of 10ppm to 4oppm at room temperature.

Conclusions

The results obtained from this research represent a qualitative addition to improving the performance of gas sensors fabricated from a PS layer. The incorporation of gold nanoparticles into PS significantly increases the sensitivity and reduces the response and recovery times, thus increasing the speed of the gas sensor. The incorporating of the AuNPs through the dipping process of porous silicon in an aqueous gold salt solution is an effective method modifying the morphological and topographical properties of the formed layer. This plays a very important role in improving the degassing properties by increasing the electrical and thermal conductivities within the porous silicon layer, which leads to a reduction in the condensation rate of gas molecules within the pores.

Acknowledgements

The authors are thankful for the support of Mustansiriyah University – Baghdad – Iraq (www.uomustansiriyah.edu.iq).

References

[1] Rashid, RB AM Alwan, A. D. “Novel approach of laser formation and characterization of multi-faceted bi-lateral/front continuous PSi layeNo Title,” *Appl. Phys. A*, vol. 130, 2024.

[2] Rashid, R. B., Alwan, A., & M. “Room temperature 2-fold morphology porous silicon impedance matching pesticide sensorNo Title,” *Appl. Sci. Nanotechnol*, vol. 3, 2023.

[3] Hashim, I. H., Hadi, H. A., & Hayif, N. D. H. “Non-thermal atmospheric jet plasma effects on the morphological, electrical and optical properties of nanocrystalline siliconNo Title,” *Mustansiriyah J. Pure Appl. Sci.*, vol. 2, pp. 93–103, 2024.

[4] M. Hernández-Montelongo, J., Muñoz-Noval, A., García-Ruíz, J. P., Torres-Costa, V., Martín-Palma, R. J., & Manso-Silván, “Nanostructured porous silicon: the winding road from photonics to cell scaffolds–a review.No Title,” *Front. Bioeng. Biotechnol.*, vol. 3, 2015.

[5] Hayif, N. D., Hadi, H. A., & Hashim, I. H. “Enhancement of Performance Au/PSi/n-Si/Ag Heterojunction Photodetector by Non-thermal Plasma No Title,” *Silicon*, vol. 17, pp. 531–554, 2025.

[6] Hadi, Hasan A., Raid A. Ismail, and A. R. A. “Effect of gamma irradiation on the optoelectronics properties of porous Si/c-Si heterojunction photodetectorNo Title,” *Silicon*, vol. 16, pp. 1097–1106, 2024.

[7] F. Ledoux, G., Gong, J., & Huisken, “Effect of passivation and aging on the photoluminescence of silicon nanocrystals,",” *Appl. Phys. Lett.*, vol. 79, pp. 4028–4030, 2001.

[8] A. M. Alwan, A. A. Yousif, and L. A. Wali, “The growth of the silver nanoparticles on the mesoporous silicon and macroporous silicon: a comparative study,” 2017.

[9] Hadi, H. A., & Hashim, I. H. “Electrical properties and schematic band diagrams of Sn/PS/p-

Si heterojunction," *J. Electron Devices*, vol. 20, pp. 1701–1710, 2014.
[10] H. F. Hussein, M. J., Yunus, W. M. M., Kamari, H. M., Zakaria, A., & Oleiw, "Effect of current density and etching time on photoluminescence and energy band gap of p-type porous silicon," *Opt. Quantum Electron.*, vol. 48, pp. 1–8, 2016.
[11] S. Gurunathan, J. Han, J. H. Park, and J.-H. Kim, "A green chemistry approach for synthesizing biocompatible gold nanoparticles," *Nanoscale Res. Lett.*, vol. 9, no. 1, p. 248, 2014.
[12] H. Y. and R. A. Tengku Sarah Tengku Amran , Md Roslan Hashim , Nihad K Ali Al-Obaidi, "Optical absorption and photoluminescence studies of gold nanoparticles deposited on porous silicon," *Nanoscale Res. Lett. Springer*, vol. 8, 2013.
[13] C. Tsai *et al.*, "Thermal treatment studies of the photoluminescence intensity of porous silicon," *Appl. Phys. Lett.*, vol. 59, no. 22, pp. 2814–2816, 1991.
[14] M. Jeske, J. W. Schultze, M. Thönissen, and H. Münder, "Electrodeposition of metals into porous silicon," *Thin Solid Films*, vol. 255, no. 1–2, pp. 63–66, 1995.
[15] S. A. Gösele U, Frank W, "Mechanism and kinetics of the diffusion of gold in silicon," *Appl Phys Mater Sci Process*, vol. 23, pp. 361–368, 1980.
[16] A. M. Alwan, R. B. Rashid, and A. B. Dheyab, "Morphological and electrical properties of gold nanoparticles /macroPorous silicon for CO2 gas," *Iraqi J. Sci.*, vol. 59, no. 1 A, pp. 57–66, 2018, doi: 10.24996/IJS.2018.59.1A.8.
[17] L. Z. Zheng J, Zhu Z, Chen H, "Nanopatterned assembling of colloidal gold nanoparticles on silicon," *Langmuir*, vol. 16, pp. 4409–4412, 2000.
[18] F. D. Mendes PM, Jacke S, Critchley K, Plaza J, Chen Y, Nikitin K, Palmer RE, Preece JA, Evans SD, "Gold nanoparticle patterning of silicon wafers using chemical e-beam lithography," *Langmuir*, vol. 20, pp. 3766–3768, 2004.
[19] Y. A. Huang, Y.; Luo, Y.; Liu, H.; Lu, X.; Zhao, J.; Lei, "Subcutaneously Injected SERS Nanosensor Enabled Long-term in Vivo Glucose Trackingm," *Eng. Sci*, vol. 14, pp. 59–68, 2020.
[20] Y. Fan, Z. Chen, J. Liang, Y. Wang, and H. Chen, "Preparation of superhydrophobic films on copper substrate for corrosion protection," *Surf. Coatings Technol.*, vol. 244, pp. 1–8, 2014, doi: 10.1016/j.surfcoat.2014.01.005.
[21] H. Mhamdi *et al.*, "Room temperature NO2 gas sensor based on stain-etched porous silicon: Towards a low-cost gas sensor integrated on silicon," *Inorg. Chem. Commun.*, vol. 139, p. 109325, 2022.
[22] and W. D. Azaiez, Khaoula, Hela Mhamdi, Rabia Benabderrahmane Zaghouani, Tomas Fiorido, Jean-Louis Lazzari, Marc Bendahan, "Investigation of a sensitive, selective and cost-effective electrochemical meso-porous silicon based gas sensor for NO2 detection at room temperature.," *he Eur. Phys. J. Appl. Phys.*, vol. 99, 2024.
[23] M. Sainato, L. M. Strambini, S. Rella, E. Mazzotta, and G. Barillaro, "Sub-parts per million NO2 chemi-transistor sensors based on composite porous silicon/gold nanostructures prepared by metal-assisted etching," *ACS Appl. Mater. Interfaces*, vol. 7, no. 13, pp. 7136–7145, 2015.
[24] B. G. Rasheed and M. A. Ibrahem, "Laser micro/nano machining of silicon," *Micron*, vol. 140, p. 102958, 2021, doi: 10.1016/j.micron.2020.102958.
[25] W. Herth, E., Zeggari, R., Rauch, J. Y., Remy-Martin, F., & Boireau, "Investigation of amorphous SiOx layer on gold surface for Surface Plasmon Resonance measurements," *Microelectron. Eng.*, vol. 163, pp. 43–48, 2016.
[26] N. F. Hadi, H. A., Kasim, S. T., Farhan, F. K., Ismail, R. A., & Habubi, "Effect of porosity on thermal properties of porous silicon," *Silicon*, vol. 15, pp. 2715–2725, 2023.
[27] A. A. Y. and layla A. W. Alwan M. Alwan, "The growth of the silver nanoparticles on the mesosilicon and macrosilicon: A comparative study," *Indian J. pure& Appl. Phys.*, vol. 55, pp. 513–520, 2017.
[28] A. J. hayder and A. a. J. Alwan M. Alwan, "Study om morphological and structural

properties of silver plating on laser etched silicon," *Surf. Coat. Technol.*, vol. 283, pp. 22–28, 2015.

[29] Alwan M. Alwan and Amer B. Dheyab, "Room temperature CO2 gas sensors of AuNPs/mesoPSi hybrid structures," *Appl Nanosci*, 2017.

[30] T. and H. Latefa Baba Ahmeda, Sabrina Naamab, Aissa Keffousb, Abdel kader Hassein-Beya, "H2 sensing properties of modified silicon nanowires," *Prog. Nat. Sci. Int.*, vol. 25, pp. 101–110, 2015.

[31] N. D. Hayif, H. A. Hadi, and I. H. Hashim, "Enhancing the gas sensing of porous silicon by surface modification using non-thermal plasma," *J. Mater. Sci. Mater. Electron.*, vol. 36, no. 13, pp. 1–21, 2025.

[32] J. H. Adawyia, M. A. Alwan, and A. J. Allaa, "Optimizing of porous silicon morphology for synthesis of silver nanoparticles," *Microporous Mesoporous Mater.*, vol. 227, pp. 152–160, 2016.

[33] H. R. Abed, A. I. Khudadad, and F. M. Oleiwi, "Influence of the distance between nozzle and substrate on the structural, photoluminescence, and detector characteristics of p-NiO/n-Si hetero-junction deposited by spray pyrolysis method," *Opt. Quantum Electron.*, vol. 54, no. 8, p. 482, 2022.

[34] A. S. Abdulhameed, H. A. Hadi, and R. A. Ismail, "Structural and optical properties of black silicon prepared by wet chemical etching," *Mustansiriyah J. Pure Appl. Sci.*, vol. 3, no. 1, pp. 123–134, 2025.

[35] S. I. Kurganskii, O. A. Dezhina, M. D. Manyakin, E. V Parinova, D. A. Koyuda, and S. Y. Turishchev, "Natural surface oxidation consideration in first principles modeling of the X-ray absorption near edge fine structure of silicon," *Results Phys.*, vol. 21, p. 103778, 2021.

[36] A. Rosyidah *et al.*, "Eco-friendly synthesis of gold nanoparticles by marine microalgae Synechococcus moorigangae: Characterization, antimicrobial, and antioxidant properties," *Kuwait J. Sci.*, vol. 51, no. 2, p. 100194, 2024.

[37] P. S. Prevéy, "X-ray diffraction residual stress techniques," 1986.

[38] S. Bykkam, M. Ahmadipour, S. Narisngam, V. R. Kalagadda, and S. C. Chidurala, "Extensive studies on X-ray diffraction of green synthesized silver nanoparticles," *Adv. Nanopart*, vol. 4, no. 1, pp. 1–10, 2015.

[39] C. Matei Ghimbeu, J. Schoonman, M. Lumbreras, and M. Siadat, "Electrostatic spray deposited zinc oxide films for gas sensor applications," *Appl. Surf. Sci.*, vol. 253, pp. 7483–7489, 2007.

[40] R. Suryana and N. Q. Aini, "Analysis of porous silicon formation on N-type Si (100) using laser-assisted electrochemical anodization method," *J. Phys. its Appl.*, vol. 4, no. 2, pp. 28–32, 2022.

[41] A. A. Yousif, H. R. Abed, and A. M. Alwan, "Different Electrode Configurations for NH3 Gas Sensing Based on Macro Porous Silicon Layer," *Silicon*, vol. 14, no. 7, pp. 3269–3280, 2022, doi: 10.1007/s12633-021-01058-8.